Electronic Supplementary Information

Self-Growth-Templating Synthesis of 3D N,P,Co-Doped Mesoporous Carbon Frameworks for Efficient Bifunctional Oxygen and Carbon Dioxide Electroreduction

Fuping Pan,[a,b] Aimin Liang,[a] Youxin Duan,[a] Qiao Liu,[c] Junyan Zhang,*[a] Ying Li,*[b]

[a] State Key Laboratory of Solid Lubrication, Lanzhou Institute of Chemical Physics, Chinese Academy of Science, Lanzhou 730000, China

[b] Department of Mechanical Engineering, Texas A&M University, College Station, TX 77843, USA

[c] Institute of Materials, Ningbo University of Technology, Ningbo 315016, China

Corresponding Author

*E-mail: zhangjunyan@licp.cas.cn; yingli@tamu.edu

Physical Characterization. The morphology, structure and compositions of MPCs were characterized by field emission scanning electron microscopy (FE-SEM, SU8020), transmission electron microscopy (TEM, TECNAI G2 TF20), X-ray diffraction (XRD, X' PERT P RO), X-ray photoelectron spectroscopy (XPS, ESCALAB 250Xi), Raman spectrometer (LabRAM ARAMIS, Horiba Jobin Yvon), N_2 adsorption-desorption tests (ASAP 2020), thermal gravimetric analysis (TGA, DSC200F3).

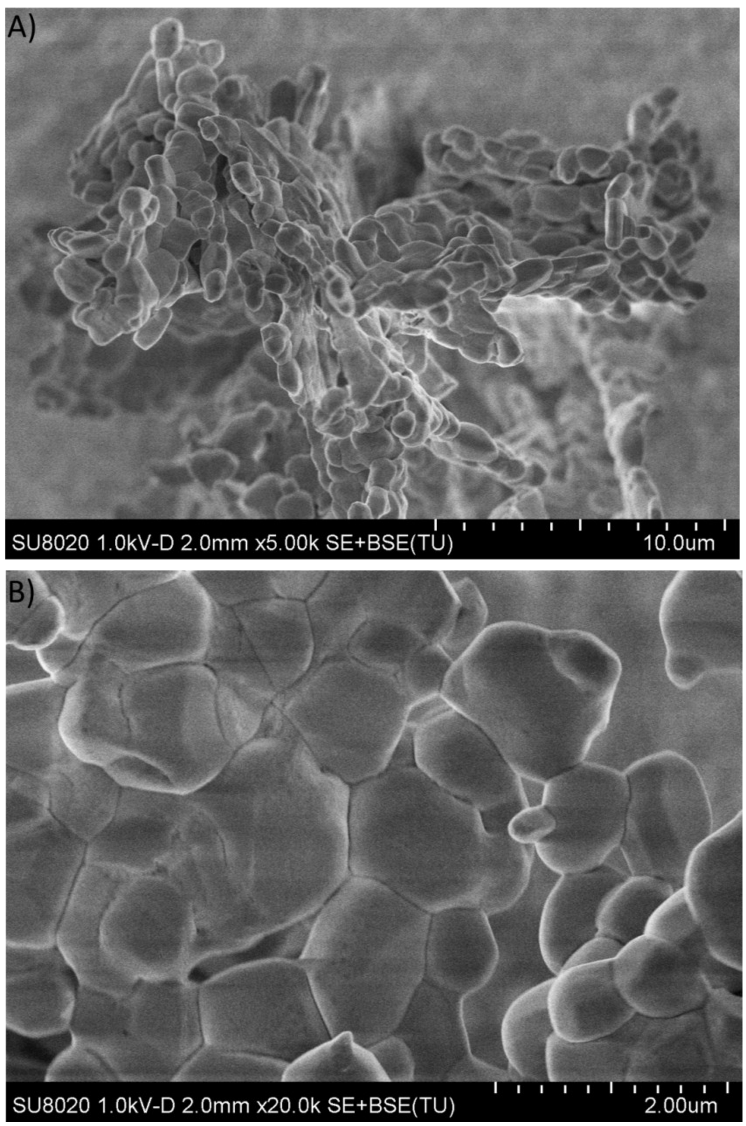

Fig. S1 Typical SEM images of freeze-dried VB-NaCl assemble.

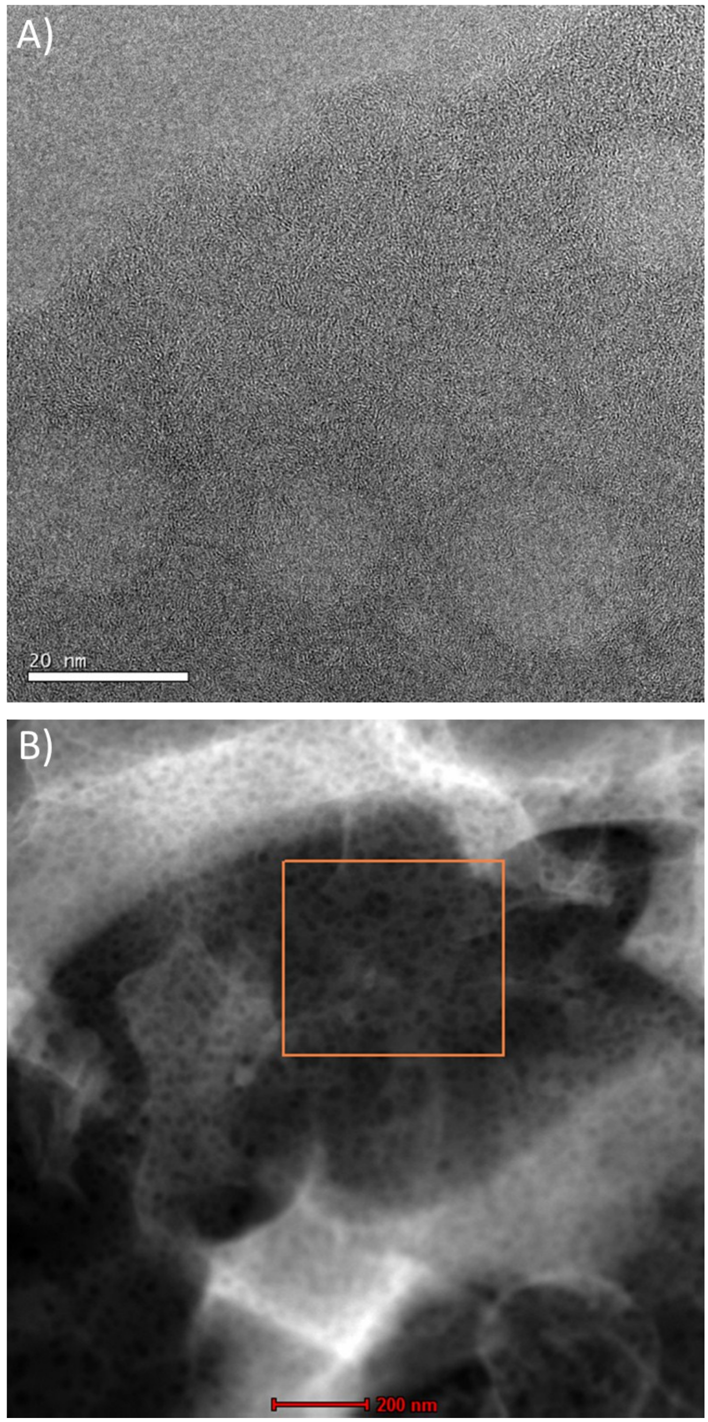

Fig. S2 A) Magnified TEM image and B) STEM image of MPC-900.

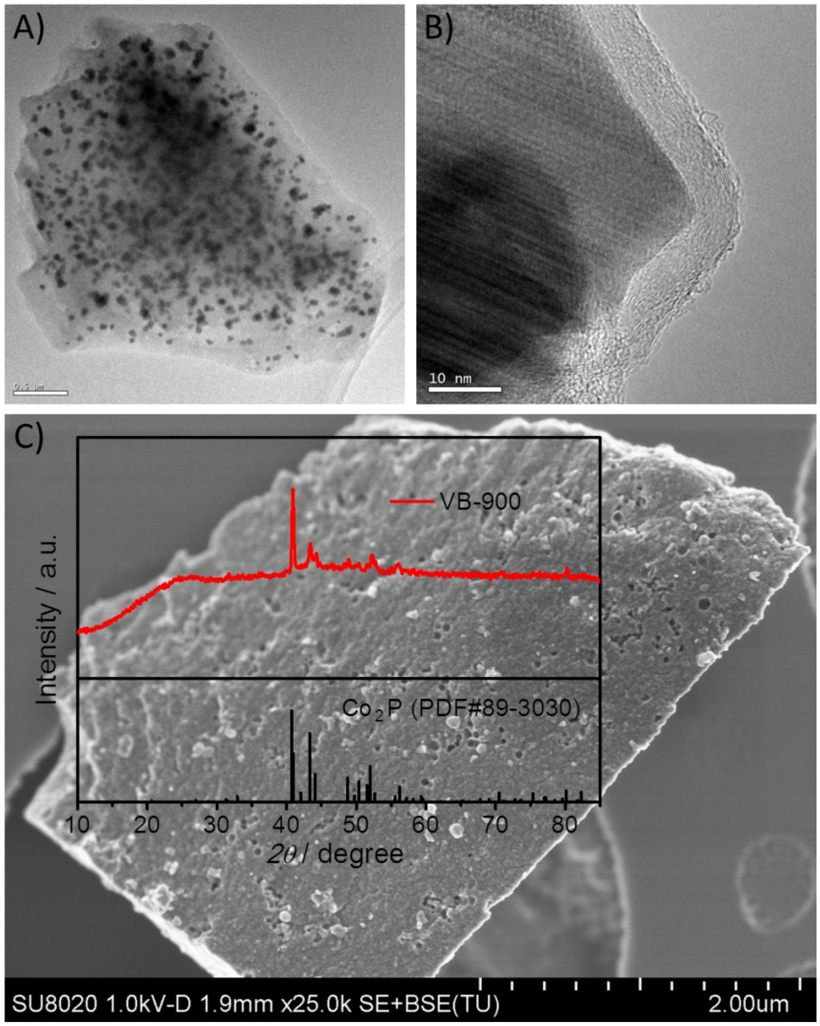

Fig. S3 A) TEM, B) HRTEM and C) SEM images of VB-900. Insert of C) is XRD pattern of VB-900.

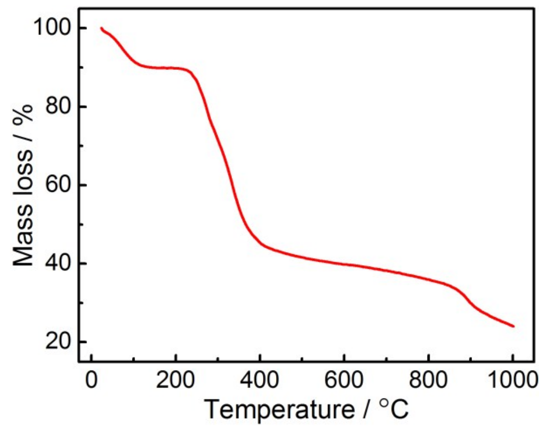

Fig. S4 TGA characterization of VB12 after lyophilization of water.

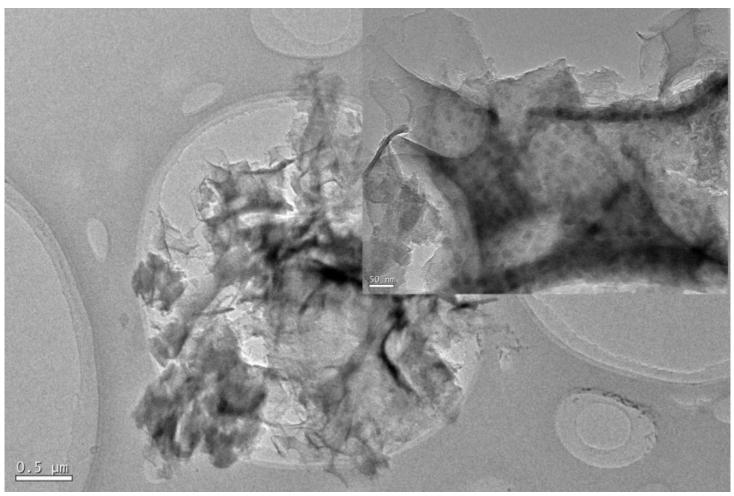

Fig. S5 TEM image of VB-Na-400.

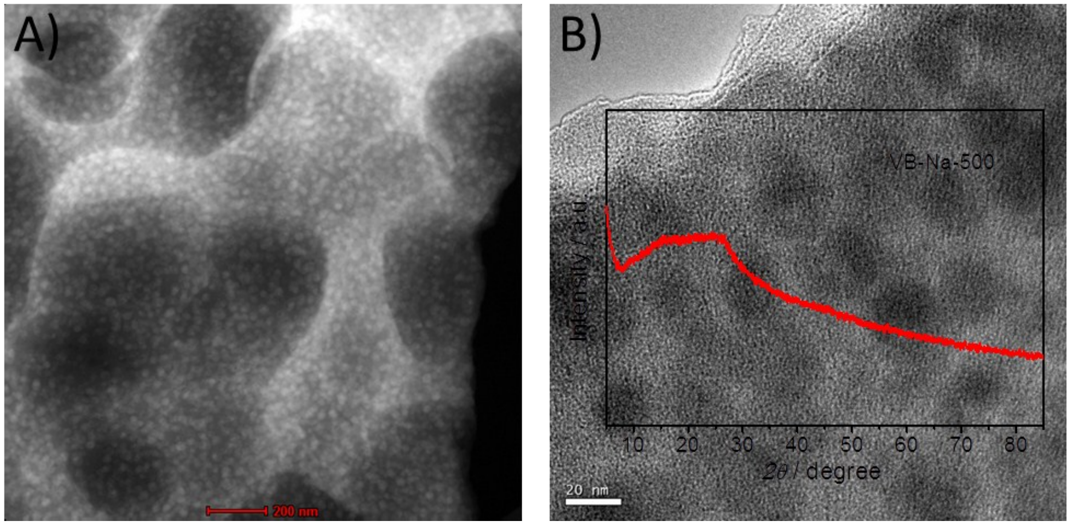

Fig. S6 A) STEM and B) TEM images of VB-Na-500. Insert of B) is the XRD pattern of VB-Na-500.

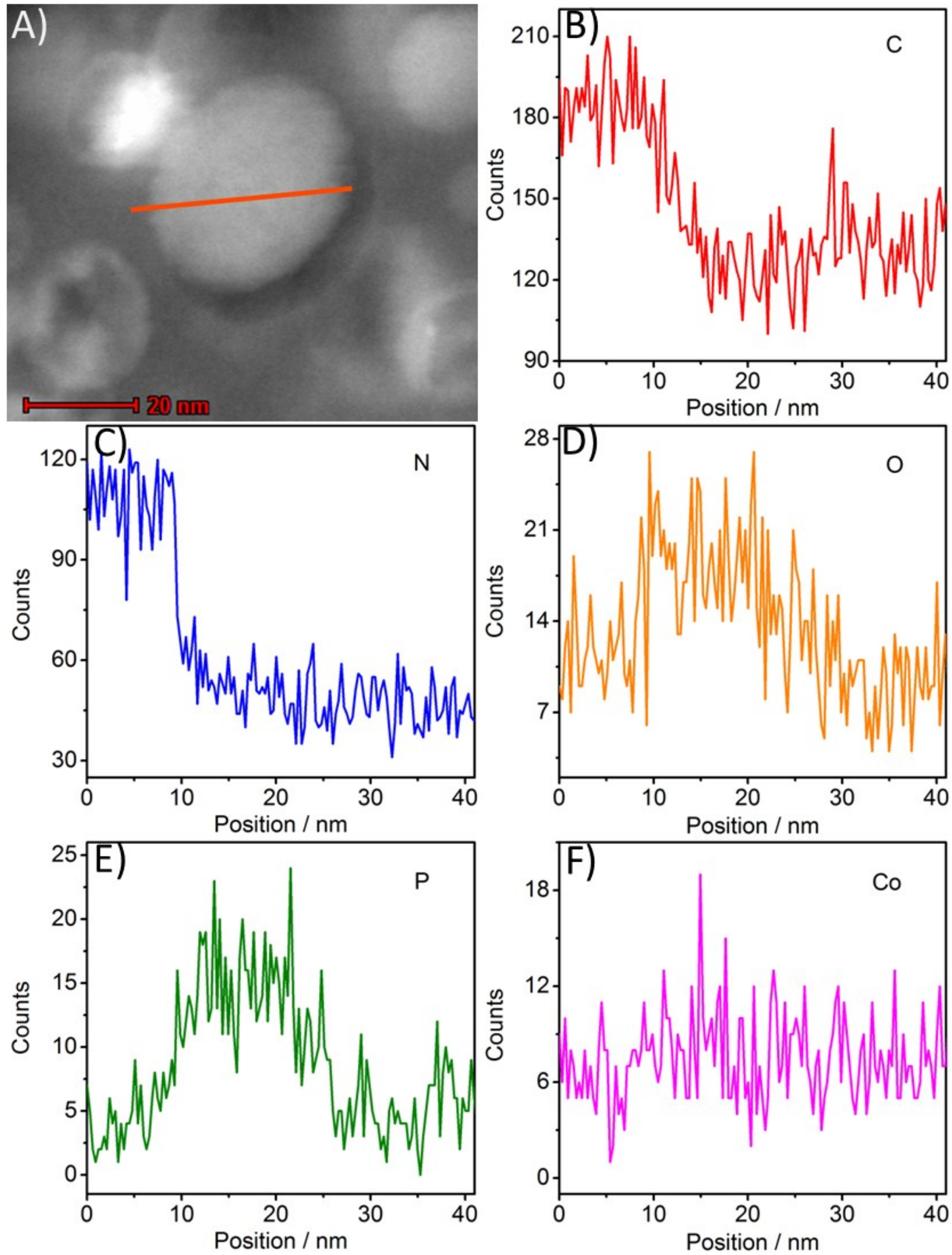

Fig. S7 A) STEM image of VB-Na-500. B-F) The C, N, O, P and Co elemental-linear images of the orange line in A).

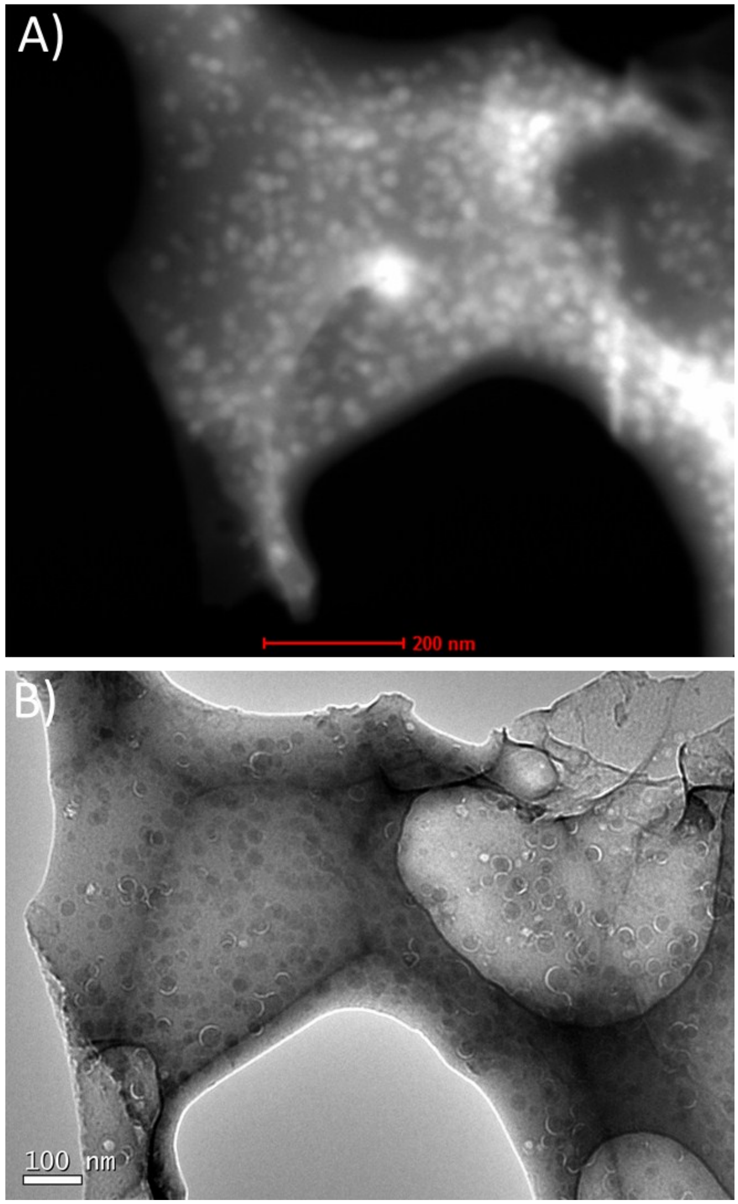

Fig. S8 TEM image of VB-Na-600.

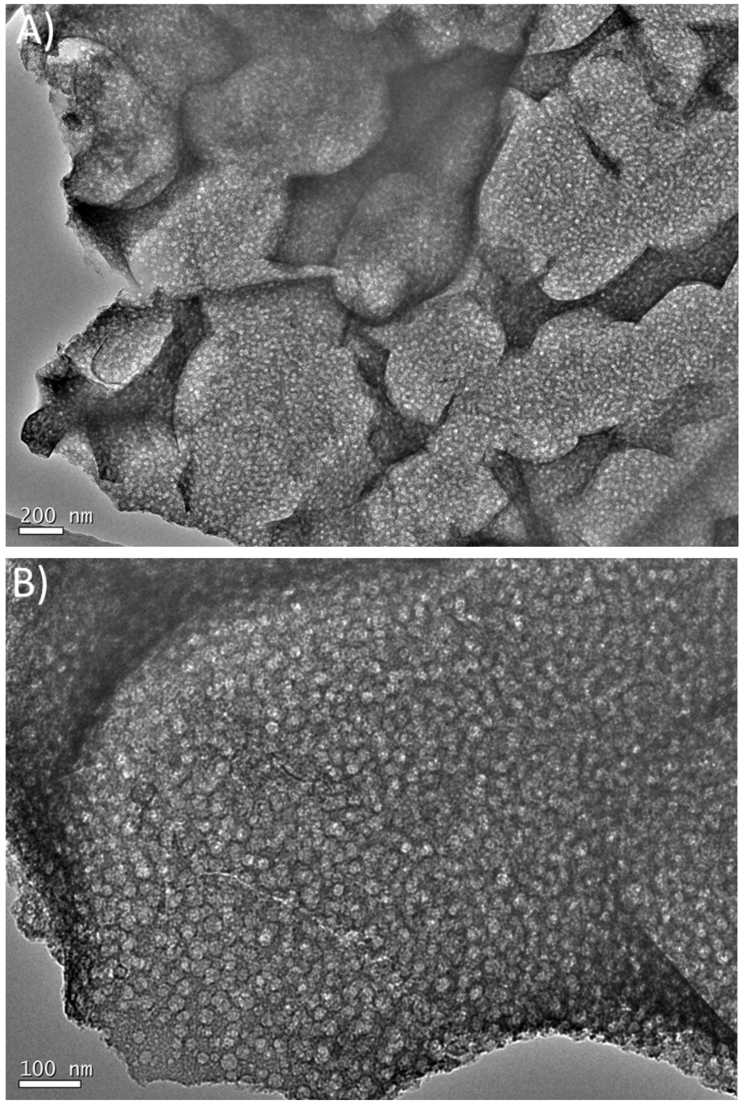

Fig. S9 A) TEM and B) magnified TEM images of MPC-700.

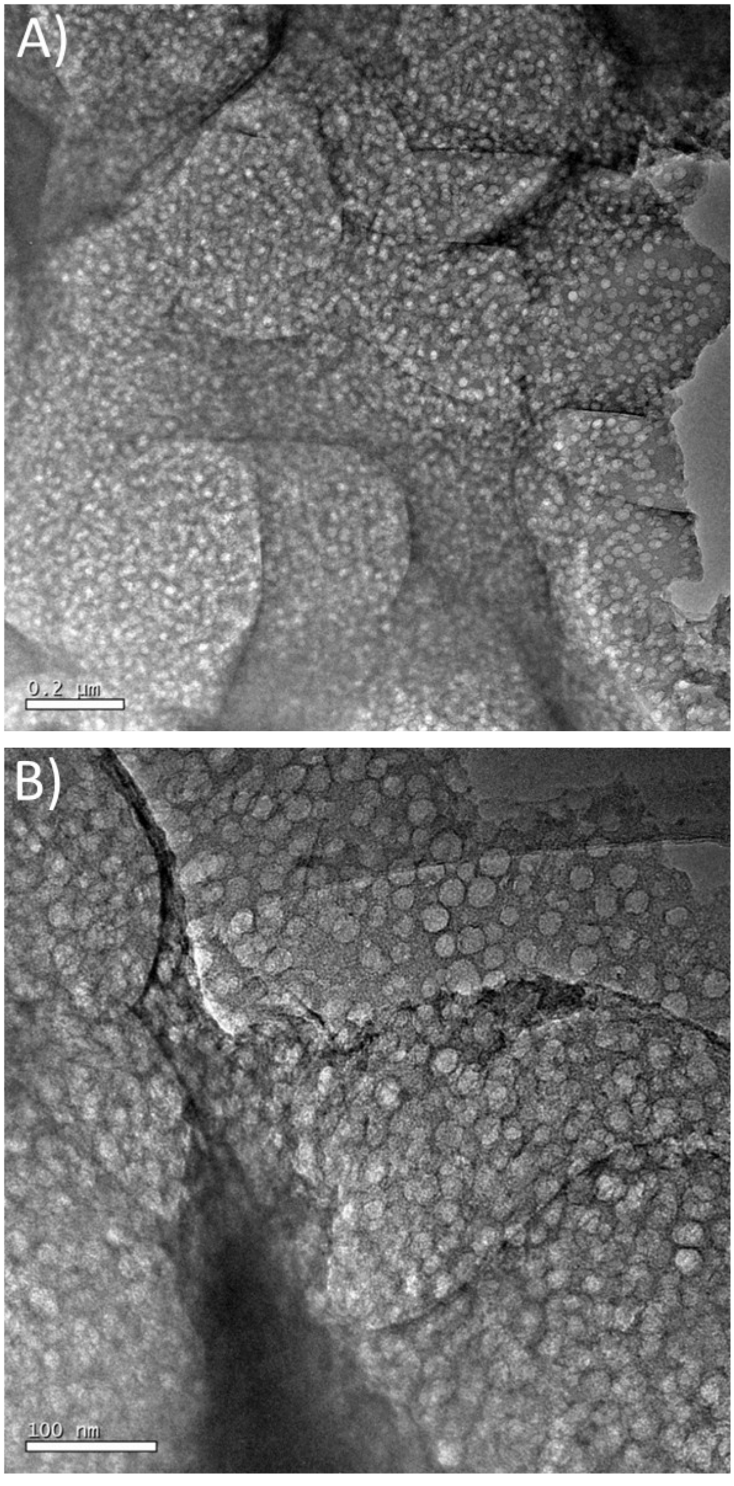

Fig. S10 A) TEM and B) magnified TEM images of MPC-800.

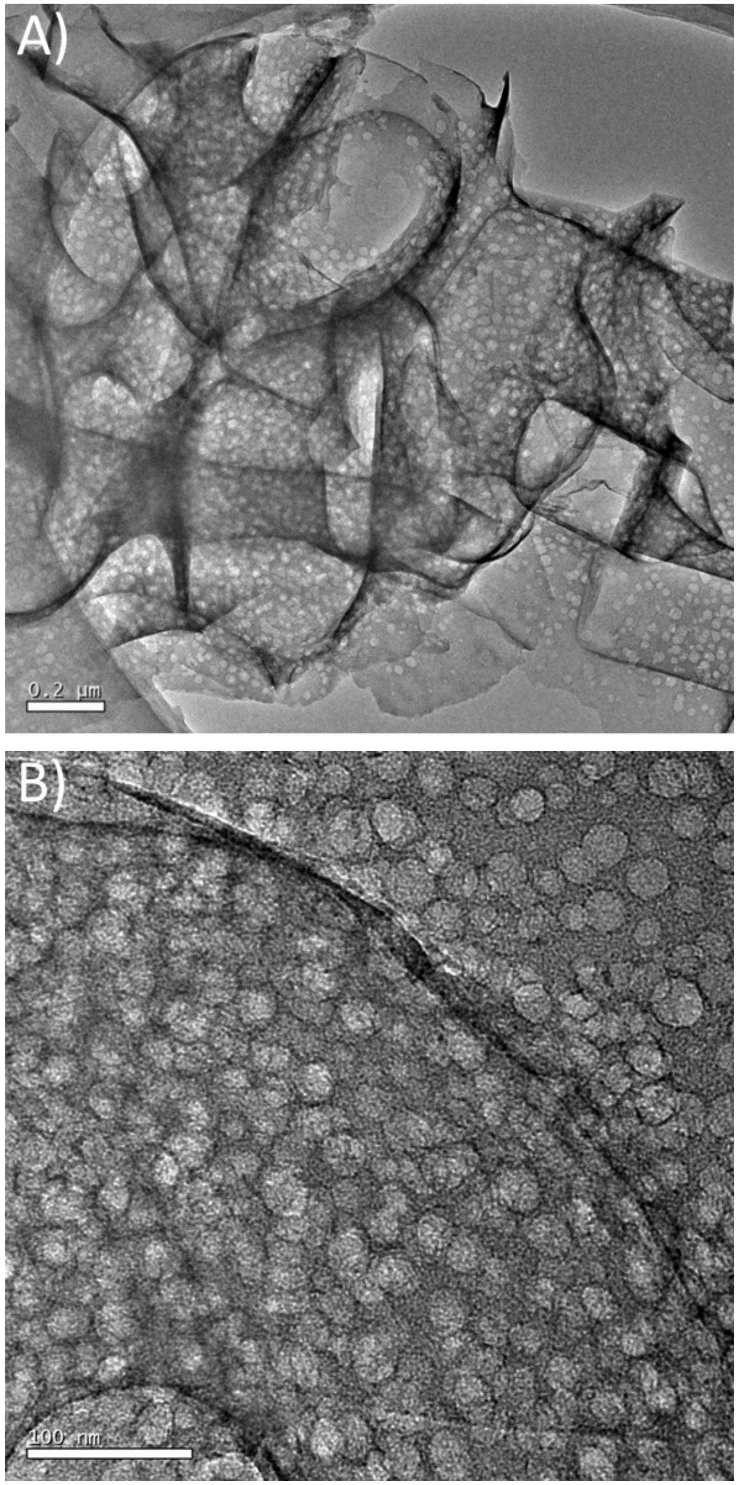

Fig. S11 A) TEM and B) magnified TEM images of MPC-1000.

Table S1 Summary of synthesis parameters and texture properties of samples.

Sample	Feedstock used	Pyrolysis temp. (ºC)	BET surface area (m^2 g^{-1})	Pore volume (cm^3 g^{-1})
VB-900	Vitamin B_{12}	900	24	0.04
VB-Na-500	Vitamin B_{12}+NaCl	500	201	0.22
VB-Na-600	Vitamin B_{12}+NaCl	600	228	0.28
MPC-700	Vitamin B_{12}+NaCl	700	356	0.67
MPC-800	Vitamin B_{12}+NaCl	800	626	1.28
MPC-900	Vitamin B_{12}+NaCl	900	779	1.86
MPC-1000	Vitamin B_{12}+NaCl	1000	1036	2.55

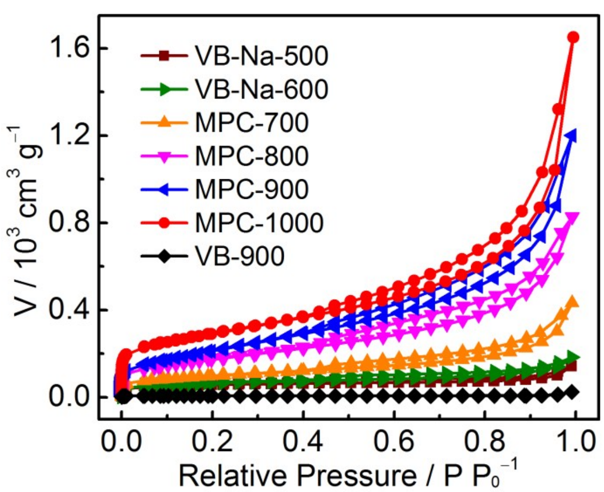

Fig. S12 N_2 adsorption/desorption isotherms and VB-900, VB-Na-X and MPCs.

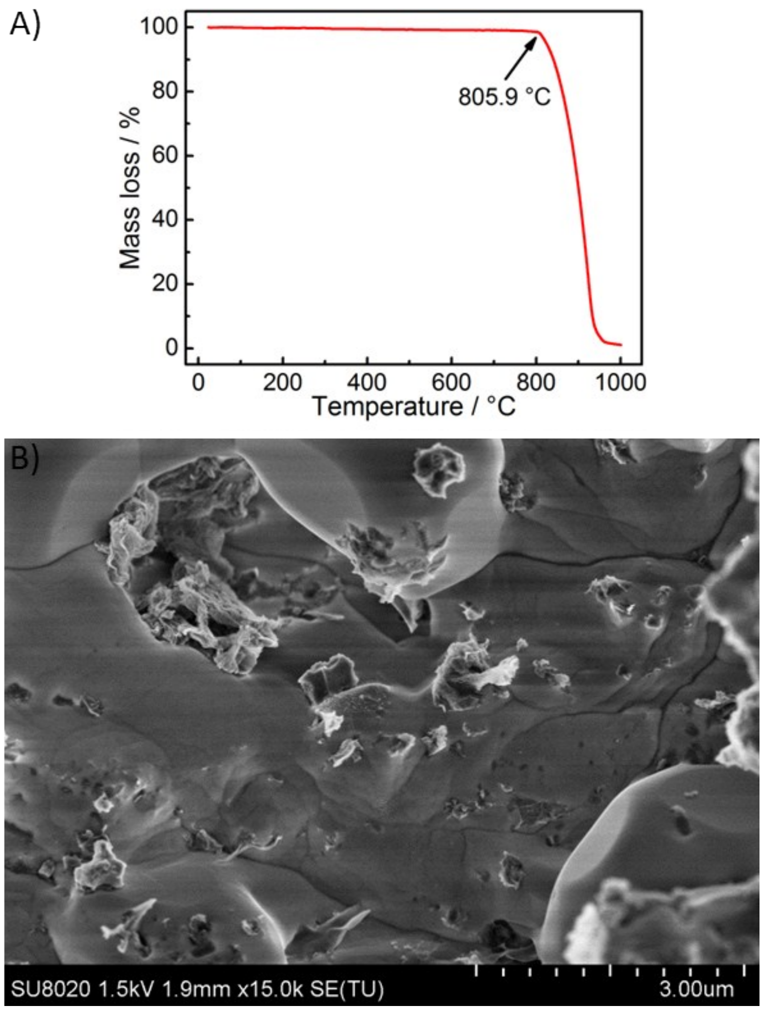

Fig. S13 A) TGA curve of VB-NaCl. B) SEM image and photograph (inset of B) of MPC-900 before removing of NaCl. This morphology indicates that MPC-900 is sealed inside in NaCl molten salts.

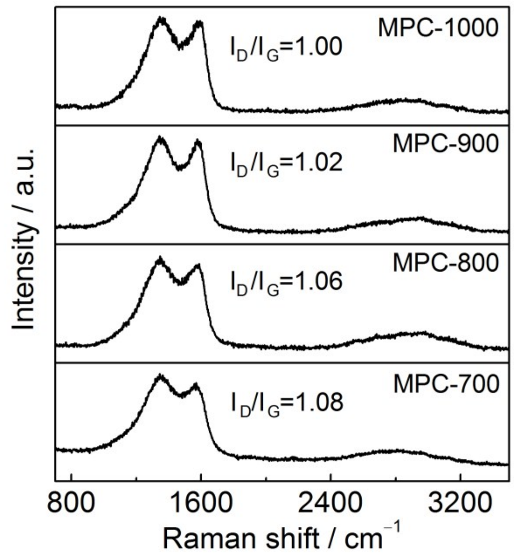

Fig. S14 Raman spectra of MPCs. It is observed that the value of ID/IG for MPCs decrease significantly when annealing temperature above 900 ºC, suggesting that the graphitization degree is enhanced.

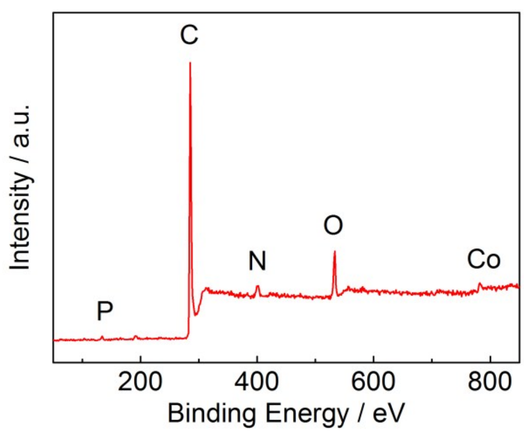

Fig. S15 XPS survey spectra of MPC-900.

Table S2 Summary of elemental contents for MPCs and VB-900.

	VB-900	MPC-700	MPC-800	MPC-900	MPC-1000
Total P (at.%)	1.21	1.47	1.38	1.31	0.98
P−C (at.%)		0.55	0.99	1.00	0.72
P−O (at.%)		0.92	0.39	0.31	0.26
Total N (at.%)	1.36	10.19	7.17	4.58	2.68
Pyridinic N (at.%)		4.87	3.68	1.94	0.88
Pyrrolic N (at.%)		2.49	1.10	0.50	0.22
Graphitic N (at.%)		1.84	1.87	1.80	1.32
Oxidized N (at.%)		0.99	0.52	0.34	0.26
Total Co (at.%)	0.59	1.17	1.03	0.74	0.45

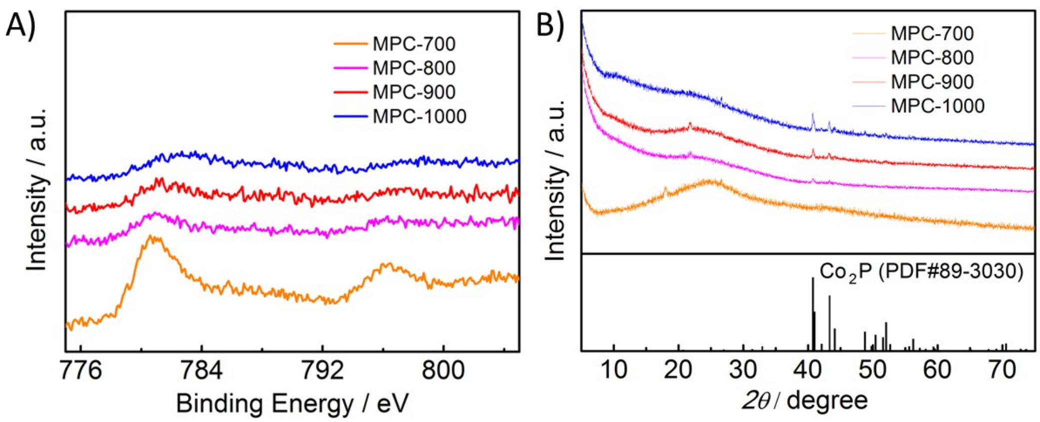

Fig. S16 A) Co 2p XPS and B) XRD spectra of MPCs.

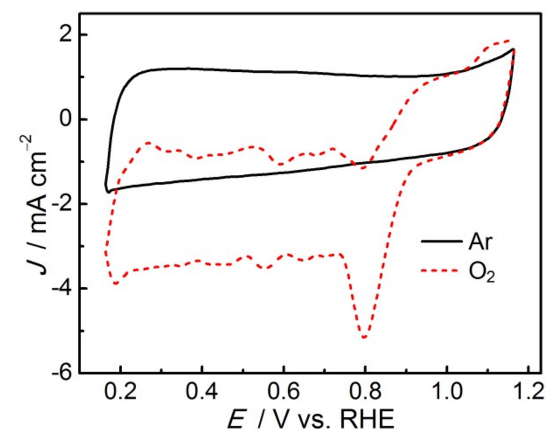

Fig. S17 CV curves of MPC-900 in Ar- and O_2-saturated 0.1 M KOH aqueous solution with a scan rate of 50 mV s^{-1}.

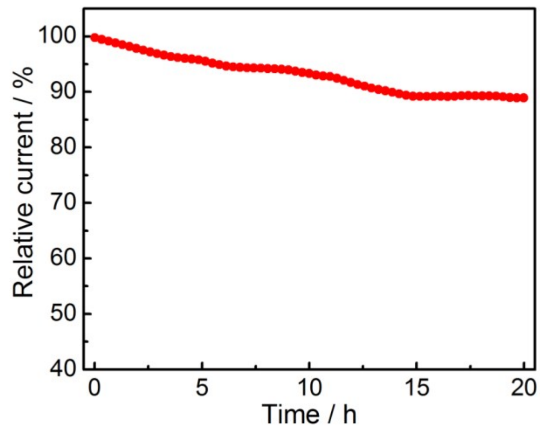

Fig. S18 Chronoamperometric responses for ORR durability evaluation on MPC-900 electrode with the rotation rate of 1600 rpm at 0.76 V in O_2-saturated 0.1 M KOH solution.

Table S3 Comparison of ORR catalytic performances under alkaline conditions between MPC-900 and porous carbon-based catalysts in previous reports.

Catalysts	CV peak potential	Half-wave potential	Electron transferred number	References
MPC-900	−0.16 V (vs. Ag/AgCl) 0.80 V (vs. RHE)	−0.11 V (vs. Ag/AgCl) 0.85 V (vs. RHE) (1600 rpm)	3.8	This work
N-doped porous carbon	-	0.87 V (vs. RHE)	3.97	Nat. Commun. 2014, 5, 4973
S-Doped	–0.34 V	–0.37 V	3.13	Angew. Chem. 2015,

Graphene	(vs. SCE)			127, 1908-1912
B-doped Graphene	−0.18 V (Ag/AgCl)	−0.175 V	4.16	Green Chem. 2015, 17, 3552-3560
P-doped Graphene	0.6 V (vs. RHE)	0.58 V	3.8	Adv. Mater. 2013, 25, 4932-4937
N,S-Codoped Carbon	−0.22 V (vs. Ag/AgCl)	~ −0.24 V	3.4	ChemSusChem 2015, 8, 1608-1617
N,P,S-doped porous carbon	−0.20 V (vs. Ag/AgCl)	−0.19 V	3.6	Sci. Rep. 2014, 4, 5130
N,P-codoped carbon tube	-	0.79 V (vs. RHE)	3.97	J. Mater. Chem. A 2014, 2, 15448-15453
N, P-codoped porous carbon	−0.22 V (vs. Ag/AgCl)	−0.19 V	3.96	Chem. Eur. J. 2014, 20, 3106-3112
N, P-codoped biocarbon	-	0.82 V (vs. RHE)	3.8	ACS Catal. 2015, 5, 920-927
N,P-codoped graphene/car bon nanosheets	0.85 V (vs. RHE)	0.83 V	-	ACS Catal. 2015, 5, 4133-4142
Porous N,P-	−0.17 V	−0.21 V	3.7	Appl. Catal. B: Environ.

doped carbon	(vs. Ag/AgCl)	(vs. Ag/AgCl)		2017, 204, 394-402
NFe-doped carbon	0.85 V (RHE)	0.90 V	3.9	Angew. Chem. Int. Edit. 2017, 56, 1-6
N,Co-doped porous carbon	0.86 (RHE)	0.87	4	Adv. Energy Mater. 2017, 7, 1601979
g-C_3N_4/C	−0.3 V (vs. Ag/AgCl)	~ −0.29 V (1500 rpm)	3	Angew. Chem. Int. Edit. 2012, 51, 3892-3896
N-S-G	−0.24 V (vs. Ag/AgCl)	~ −0.36 V (1600 rpm)	3.6	Angew. Chem. Int. Edit. 2012, 51, 11496-11500.
Fe-N/C-800	0.81 V (vs. RHE)	0.80 V (1600 rpm)	3.95	J. Am. Chem. Soc. 2015, 137, 5555-5562
Meso/micro-PoPD	0.83 V (vs. RHE)	0.87 V (1600 rpm)	3.97	Nat. Commun. 2014, 5, 4973
Co@Co_3O_4 @C-CM	0.79 V (vs. RHE)	0.81 V (1600 rpm)	3.9	Energy Environ. Sci. 2015, 8, 568-576
NSC-800	-	0.74 V (vs. RHE) (1600 rpm)	4	Energy Environ. Sci. 2014, 7, 4095-4103
NOSCs	0.75 V (vs. RHE)	~0.74 V (1600 rpm)	4	J. Am. Chem. Soc. 2014, 136, 13554-13557
Fe-N/MCNs	0.82 V	0.83 V	4	Nanoscale 2015, 7,

	(vs.RHE)	(1600 rpm)		6247-6254
NMCS-3	−0.21 V (vs. Ag/AgCl)	−0.23 V (1600 rpm)	-	Angew. Chem. Int. Edit. 2015, 54, 588-593
N-OMMC-G	−0.28 V (vs. Ag/AgCl)	−0.23 V (1600 rpm)	-	Adv. Mater. 2013, 25, 6226-6231

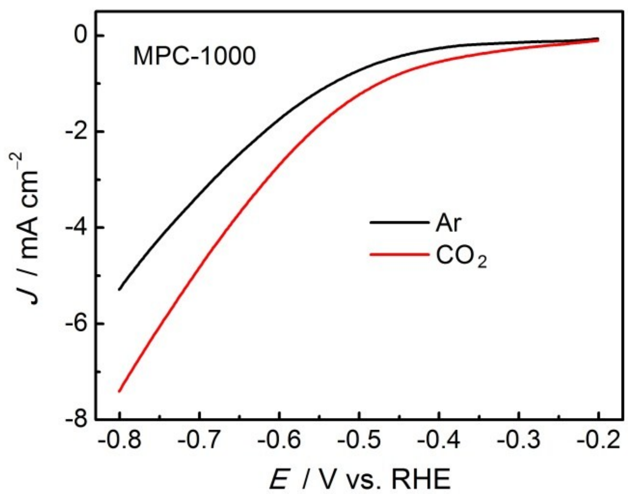

Fig. S19 LSV curves of MPC-1000 in Ar- and CO_2-staurated 0.1 M $KHCO_3$ solution with scan rate of 5 mV s^{-1}.

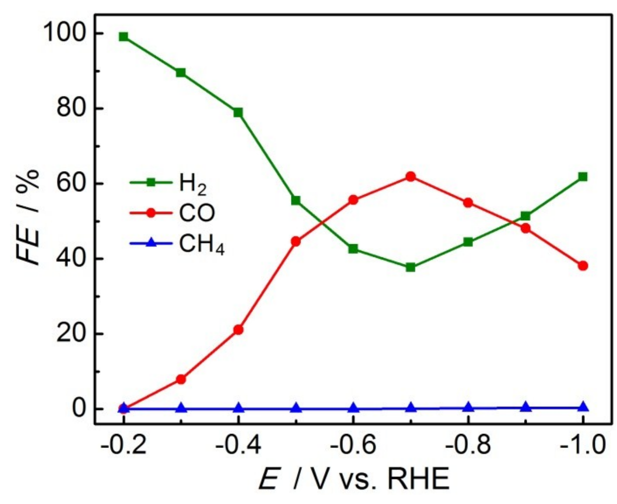

Fig. S20 FE of MPC-1000 for H_2, CO, and CH_4 at different applied potentials in CO_2-staurated 0.1 M $KHCO_3$.

Table S4 Comparison of CO2RR performances for CO production between MPC-1000 and reported carbon-based catalysts and noble metal.

Catalysts	FE and J_{CO}[a] (mA cm^{-2})	Overpotential[b] (V)	Tafel slope (mV dec^{-1})	References
MPC-1000	62%, 3.1	−0.59	129	This work
N-CNT	80%, ~	−0.94	160	Angew. Chem. 2015, 127, 13905-13909
N-CNT	90%, 5.0	−0.79	126	ChemSusChem 2016, 9, 1085-1089
MOF	76%, ~1	−0.59	165	J. Am. Chem. Soc. 2015, 137, 14129-14135.
N-doped Graphene	85%, 1.8	−0.47	-	Nano Lett. 2016, 16, 466-470.
N,S-doped porous carbon	11.3%, 0.26	−0.88	-	ChemSusChem 2016, 9, 606-616.
C_3N_4/MWCNT	60%, 0.5	−0.64	-	Chem. Eur. J. 2016, 22, 11991
N-CNT	80%, 1.5	−0.69	203	ACS Nano 2015, 9, 5364.

Ag (40 nm)	75%,-	−0.6		ACS Nano 2015, 9, 5364.
Annealed Cu	45%,-	−0.24	116	J. Am. Chem. Soc. 2012, 134, 7231

[a] Partial current density for CO at which the maximum FE is obtained;

[b] Overpotential at which the maximum FE and partial current density for CO are obtained.